

Reducing Internal State in Eigenvalue-Only Divide-and-Conquer Tridiagonal Eigensolvers

Ruiyi Zhan
rui1@std.uestc.edu.cn

University of Electronic Science and Technology of China
Chengdu, China

Shaoshuai Zhang*
szhang94@uestc.edu.cn

University of Electronic Science and Technology of China
Chengdu, China

Abstract

Divide and Conquer (D&C) is a widely used algorithmic strategy for symmetric eigenvalue decomposition. Its natural parallelism makes D&C attractive on modern multicore CPUs and GPUs, but existing eigenvalue-only routines often default to QR-based methods because conventional D&C still materializes or replays large transformation matrices during the conquer phase. This paper proposes a boundary-row D&C algorithm for eigenvalue-only computation. The key observation is that the conquer phase only needs selected boundary rows/columns rather than the full accumulated eigenvector matrix. By propagating these boundary rows directly through the recursion, the proposed algorithm reduces the memory requirement from quadratic to linear space while also eliminating unnecessary matrix-vector work in the conventional lazy-replay formulation. We provide the algorithm, its time and space complexity analysis, correctness and stability arguments, optimized CPU and GPU implementations, and an evaluation against QR and D&C routines in standard numerical libraries.

1 Introduction

Symmetric eigenvalue decomposition (EVD) is a core primitive in numerical linear algebra and scientific computing. Given a real symmetric matrix $A \in \mathbb{R}^{n \times n}$, EVD computes $A = Q\Lambda Q^T$, where Λ stores the eigenvalues and Q stores the corresponding orthonormal eigenvectors. Many applications use this spectral information in quantum chemistry [17], physics [8, 16], machine learning, and signal processing [1, 11, 18, 23]. In a substantial fraction of these workloads, however, the application needs only the eigenvalues, or needs the eigenvalues before deciding whether eigenvectors are necessary. This eigenvalue-only setting changes the optimization target: the solver should not pay quadratic memory cost for eigenvector data that will not be returned.

Dense symmetric EVD is normally reduced to a tridiagonal eigenproblem before the final spectral solve. LAPACK describes the standard pipeline as first reducing A to a real symmetric tridiagonal matrix T , and then solving the tridiagonal problem for eigenvalues and, optionally, eigenvectors [2, 7]. This separation makes the tridiagonal eigensolver

a critical kernel in full EVD implementations. Once the problem reaches T , classical QR/QL routines are attractive for eigenvalue-only computation because they update only the diagonal and off-diagonal arrays and require little auxiliary storage [2, 22]. Their limitation is performance: the computation is sequential in nature and exposes much less coarse-grained parallelism than D&C.

Divide-and-conquer (D&C) is a more parallel alternative for the symmetric tridiagonal eigenproblem. Cuppen's method recursively splits T into two smaller tridiagonal matrices plus a rank-one correction, solves the child problems, and merges them by solving a secular equation [4, 9, 10, 14]. The merge has substantial parallel work across secular roots and, when eigenvectors are requested, uses matrix operations to combine child eigenvectors into the parent eigenvectors. This structure explains why production libraries include D&C drivers and why D&C can be much faster than QR for large eigensystems [2, 19]. Unfortunately, the same structure also explains why D&C is rarely the default choice for eigenvalue-only computation, because conventional D&C stores or constructs dense eigenvector information inside the recursion, leading to $O(n^2)$ space complexity. LAPACK `stedc` routine¹ also comments that the default eigenvalue-only routine is set to QR algorithm (`steqr`), due to the heavy memory cost of D&C.

The memory mismatch comes from the vector required by each rank-one merge. After splitting the tridiagonal matrix, the rank-one update is expressed in the eigenbasis of the two child subproblems. The update vector is obtained from the last row of the left child eigenvector matrix and the first row of the right child eigenvector matrix. Standard D&C therefore keeps enough child eigenvector information to produce these boundary rows at later levels. Even if the final output contains only eigenvalues, the internal algorithm still carries dense transformation data through the D&C tree. Existing lazy-replay formulations reduce unnecessary eager multiplication, but they still represent the accumulated orthogonal transformations and therefore retain a quadratic memory footprint in practical implementations.

This work asks whether eigenvalue-only D&C actually needs the dense child eigenvector matrices, and our answer

*Corresponding author.

¹https://netlib.org/lapack/explore-html/d3/d57/group__stedc_gaec55368cca7558e3ac13e04c1347bc27.html

is no. For the purpose of future D&C merges, each child sub-problem only needs to expose the boundary row or column that participates in the next rank-one update. We therefore introduce a boundary-row D&C algorithm that propagates exactly this information through the recursion. Instead of constructing or replaying the full eigenvector matrix, the algorithm updates the boundary rows needed by ancestor merges. This changes the memory behavior of eigenvalue-only D&C from storing dense intermediate transformations to storing linear-size spectral and boundary data, while preserving the same secular-equation structure as conventional D&C.

The resulting algorithm makes D&C practical for memory-constrained eigenvalue-only workloads on CPUs and GPUs. It retains the parallel merge structure that motivates D&C, but removes the main reason libraries fall back to QR-like routines when only eigenvalues are requested. The idea is especially important on GPUs, where a quadratic workspace can determine whether a large tridiagonal problem fits in device memory at all. More broadly, our work shows that the eigenvalue-only variant of D&C should not be treated as a degenerate eigenvector algorithm; it has a smaller data dependency that can be exploited directly.

The rest of the paper follows this data dependency from library behavior to algorithm, implementation, and measurement. We first review how existing tridiagonal solvers expose the QR-versus-D&C trade-off, then formalize the boundary-row state that replaces dense replay, implement the same state contract on CPU and GPU paths, and finally measure the resulting tridiagonal-stage prototypes against QR/QL, internal values-only D&C, and cuSOLVER D&C baselines.

This paper makes the following contributions:

- We identify the boundary-row dependency that causes conventional eigenvalue-only D&C to retain dense eigenvector state.
- We propose a boundary-row D&C algorithm that computes all eigenvalues of a symmetric tridiagonal matrix using linear auxiliary memory.
- We prove that the propagated boundary rows produce the same secular-equation inputs as conventional D&C and analyze the resulting time and space complexity.
- We present CPU and GPU implementations that expose D&C parallelism while avoiding full eigenvector storage.
- We evaluate CPU and GPU tridiagonal-stage prototypes against QR, internal values-only D&C, and cuSOLVER D&C routines across problem sizes and spectral structures.

2 Background and Related Work

2.1 Symmetric EVD and Tridiagonal Solvers

Dense symmetric EVD is conventionally organized as a reduction phase followed by a tridiagonal eigensolve. For a real symmetric matrix A , orthogonal transformations reduce the problem to $A = Q_A T Q_A^T$, where T is real symmetric and tridiagonal [2, 7, 21]. The eigenvalues of T are also the eigenvalues of A . If $T = Q_T \Lambda Q_T^T$ is computed, then the eigenvectors of the original dense matrix are $Q = Q_A Q_T$. This paper focuses on the tridiagonal stage, and specifically on the case where only Λ is required.

LAPACK exposes several algorithmic choices for the symmetric tridiagonal eigensolvers. The QR/QL family includes routines such as xSTERF, which computes all eigenvalues without eigenvectors using a square-root-free QR/QL variant [2, 22]. Bisection computes selected or all eigenvalues by locating roots in intervals [2, 5]. Relatively robust representations (MRRR) compute eigenpairs through carefully chosen shifted factorizations and are designed for high accuracy and low workspace [3, 6]. D&C, implemented in routines such as xSTEDC, targets all eigenvalues and eigenvectors and can be much faster than QR for large problems, but it requires substantially more workspace [2, 10].

GPU libraries expose similar choices, but their public interfaces do not provide a low-memory eigenvalue-only D&C path. NVIDIA cuSOLVER provides symmetric eigensolver routines with options for eigenvalues only and eigenpairs, and its documentation states that eigenvectors are computed by D&C when requested [15]. However, cuSOLVER is distributed as a closed-source library, so the internal eigenvalue-only path cannot be audited or modified.

MAGMA provides a source-available LAPACK-style baseline [12, 20]. Its `magma_dsyevd` and `magma_dsyevd_gpu` implementations show a sharp split. After reducing the dense matrix to tridiagonal form, `MagmaNoVec` calls LAPACK `dsterf`, whereas `MagmaVec` calls MAGMA's D&C tridiagonal solver `magma_dstedx` and then applies the accumulated transformations [13]. The workspace requirements reflect the same design choice: the eigenvalue-only path uses linear workspace for the dense reduction and QR/QL tridiagonal solve, while the eigenvector path requires quadratic workspace for the D&C eigenvector state [12, 13]. MAGMA therefore confirms the gap addressed by this paper, that D&C is available in production software, but primarily as an eigenvector-producing algorithm rather than as a low-memory eigenvalue-only algorithm.

2.2 Divide-and-Conquer for Tridiagonal EVD

D&C solves the tridiagonal eigenproblem by recursively reducing it to diagonal-plus-rank-one problems. Given an irreducible tridiagonal matrix T , the algorithm splits it at an

off-diagonal entry and writes

$$T = \begin{bmatrix} T_1 & 0 \\ 0 & T_2 \end{bmatrix} + \rho uu^T, \quad (1)$$

where T_1 and T_2 are smaller tridiagonal matrices and u has nonzeros only at the split boundary [4, 10]. If the child decompositions are

$$T_i = Q_i \Lambda_i Q_i^T, \quad i \in \{1, 2\}, \quad (2)$$

then the parent merge becomes

$$D + \rho vv^T, \quad D = \Lambda_1 \oplus \Lambda_2, \quad v = \begin{bmatrix} \pm Q_1^T e_m \\ Q_2^T e_1 \end{bmatrix}, \quad (3)$$

where $\Lambda_1 \oplus \Lambda_2$ is $\begin{bmatrix} \Lambda_1 & 0 \\ 0 & \Lambda_2 \end{bmatrix}$, $e_1 = [1, 0, \dots, 0]^T$ and $e_m = [0, \dots, 0, 1]^T$. Thus, the merge depends on the last row of Q_1 and the first row of Q_2 . The eigenvalues of the parent are then the roots of a secular equation associated with $D + \rho vv^T$ [9, 14].

After the secular equation is solved, conventional D&C constructs the parent eigenvector matrix by multiplying the block-diagonal child eigenvector matrix with the eigenvectors of the diagonal-plus-rank-one problem. This step is the source of both D&C's performance advantage and its memory cost. It uses dense matrix operations and exposes parallelism, especially near the top of the recursion tree, but it also requires dense eigenvector matrices at intermediate levels. LAPACK documentation explicitly notes that D&C can be many times faster than QR for large matrices while requiring quadratic workspace [2]. This trade-off is appropriate when eigenvectors are requested, but it is wasteful when the user asks only for eigenvalues.

2.3 Eigenvalue-Only D&C and Lazy Replay

Eigenvalue-only D&C tries to avoid forming final eigenvectors, but the merge vector v still creates an implicit dependency on child eigenvectors. A straightforward implementation can compute v by constructing child eigenvector matrices, using their boundary rows, and discarding the rest. This defeats the purpose of an eigenvalue-only routine because it stores and manipulates data whose only role is to recover a small number of rows. Lazy replay improves on this baseline by postponing the application of transformations and replaying them only when boundary information is needed. It reduces some unnecessary eager work, but the replay state still represents products of dense orthogonal transformations through the recursion. Thus lazy replay identifies the relevant dependency and reduces work relative to eagerly forming all intermediate eigenvectors, but it does not by itself give a low-memory eigenvalue-only D&C formulation.

The next section turns this dependency question into the algorithmic invariant used throughout the paper: every merge must preserve exactly the boundary information needed by future merges, and no full eigenvector block should be part of the persistent values-only state.

3 Method

The background reduces the eigenvalue-only D&C problem to a precise data-dependency question: which part of the child eigenvector basis is required by later secular merges? The key observation behind our method is that lazy replay keeps too much information for the eigenvalue-only problem. At each merge, the parent does not require the full child basis; it only requires the two boundary rows that define the secular vector. Once the secular equation has been solved, ancestors again require only boundary rows of the new parent basis. Therefore the data dependency is closed under boundary-row propagation: boundary rows of the parent can be computed from boundary rows and local merge information from the children. This observation separates eigenvalue-only D&C from full-eigenvector D&C and creates an opportunity to reduce memory from quadratic to linear.

This section turns the observation into an algorithmic invariant. It defines boundary-row state, proves that this state is sufficient to reproduce the same secular problems as conventional D&C, and derives the resulting work and storage model.

3.1 Problem Setting

The input to the tridiagonal stage is a real symmetric tridiagonal matrix $T \in \mathbb{R}^{n \times n}$. A conventional D&C merge splits T into two child tridiagonal matrices and a rank-one coupling,

$$T = \begin{bmatrix} T_L & 0 \\ 0 & T_R \end{bmatrix} + \rho uu^T, \quad (4)$$

where $T_L \in \mathbb{R}^{n_L \times n_L}$, $T_R \in \mathbb{R}^{n_R \times n_R}$, and u is nonzero only at the two split-boundary coordinates. If

$$T_L = Q_L \Lambda_L Q_L^T, \quad T_R = Q_R \Lambda_R Q_R^T, \quad (5)$$

then the parent merge is reduced to a diagonal-plus-rank-one eigenproblem

$$\begin{aligned} A_v &= \text{diag}(D) + \rho zz^T, \\ D &= \Lambda_L \oplus \Lambda_R, \\ z &= \text{concat}(\text{bhi}(Q_L), \text{blo}(Q_R)). \end{aligned} \quad (6)$$

Here $\text{blo}(Q)$ and $\text{bhi}(Q)$ denote the first and last rows of Q . The key point is that the parent secular equation needs the child spectra and only two child boundary rows; it does not need the complete child eigenvector matrices.

3.2 Boundary-Row State

BR replaces the dense eigenvector state in eigenvalue-only D&C with a boundary-row state. For each node v in the

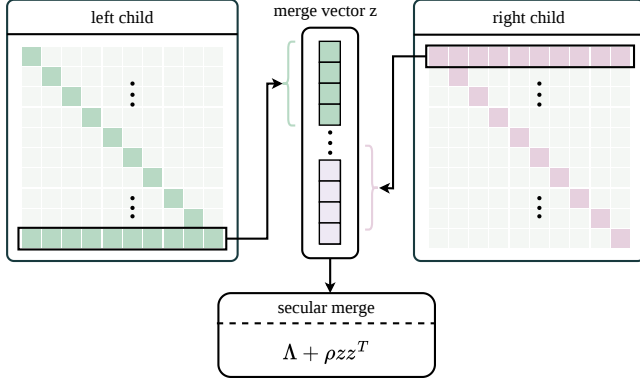


Figure 1. Data dependency of one D&C merge. The highlighted row of the left child represents $\text{bhi}(Q_L)$, and the highlighted row of the right child represents $\text{blo}(Q_R)$. Concatenating these two rows forms the secular vector z , so the merge needs only boundary rows rather than complete child eigenvector matrices.

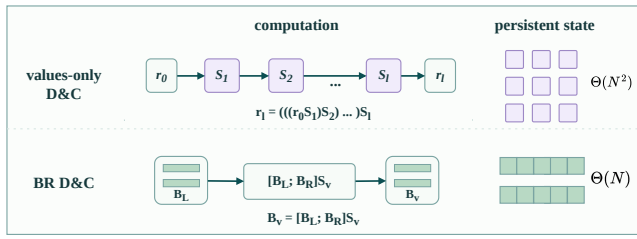


Figure 2. State and computation carried between D&C levels. The internal values-only D&C path reconstructs a requested boundary row by replaying a chain of GEMV-like transformations, $r_\ell = (((r_0 S_1) S_2) \cdots) S_\ell$, while retaining dense or replayable state with quadratic footprint. BR instead propagates boundary rows by the local recurrence $B_v = [B_L; B_R] S_v$, so only linear-size boundary state is persistent.

merge tree, let Q_v be the eigenvector matrix that conventional D&C would construct for the corresponding subproblem. BR stores

$$B_v = (\text{blo}(Q_v), \text{bhi}(Q_v)). \quad (7)$$

For an internal node, the left component required by its parent is a selected row of the parent eigenvector block; the right component is another selected row. These selected rows can be computed directly from child selected rows and the local secular-vector block, rather than by forming all rows of Q_v .

At the root, only eigenvalues are returned. Boundary rows are nevertheless propagated through internal nodes because they are the information needed by ancestor secular equations. In implementation, the requested row list σ_v contains exactly the rows demanded by ancestors and the

Algorithm 1 Boundary-row D&C for eigenvalue-only tridiagonal EVD

Input: Symmetric tridiagonal subproblem T_v and requested local rows σ_v

Output: Eigenvalues Λ_v and selected rows $(Q_v)_{\sigma_v}$

- 1: **if** T_v is a leaf problem **then**
 - 2: Solve the leaf by a small tridiagonal eigensolver.
 - 3: Return Λ_v and the requested rows of the leaf eigenvector matrix.
 - 4: **end if**
 - 5: Split T_v into left and right child problems.
 - 6: Map σ_v and split-boundary requests to child row lists σ_L, σ_R .
 - 7: Recursively compute $(\Lambda_L, (Q_L)_{\sigma_L})$ and $(\Lambda_R, (Q_R)_{\sigma_R})$.
 - 8: Form $D = \Lambda_L \oplus \Lambda_R$ and $z = \text{concat}(\text{bhi}(Q_L), \text{blo}(Q_R))$.
 - 9: Solve the local secular equations for Λ_v and the local transform S_v needed by requested rows.
 - 10: Compute $(Q_v)_{\sigma_v} = (Q_L \oplus Q_R)_{\sigma_v} S_v$ by selected-row updates.
 - 11: **return** Λ_v and $(Q_v)_{\sigma_v}$
-

split-boundary rows needed by the current parent; duplicate and unordered requests are allowed and are handled by metadata rather than by materializing full matrices.

3.2.1 Algebraic Correctness.

Lemma 3.1 (Boundary sufficiency). *For any D&C merge with child eigenvector matrices Q_L and Q_R , the secular vector z in Eq. (6) is fully determined by $\text{bhi}(Q_L)$ and $\text{blo}(Q_R)$.*

Proof. The rank-one coupling in Eq. (4) acts only on the last coordinate of the left child and the first coordinate of the right child. After transforming to the child eigenvector bases, these two coordinate vectors become $Q_L^T e_{n_L}$ and $Q_R^T e_1$. Their entries are precisely the last row of Q_L and the first row of Q_R , giving Eq. (6).

Lemma 3.2 (Selected-row multiplication). *Let $Q \in \mathbb{R}^{m \times k}$, $S \in \mathbb{R}^{k \times \ell}$, and let σ be any row list, possibly unordered and with repetitions. Then*

$$(QS)_\sigma = Q_\sigma S. \quad (8)$$

Proof. For every requested row position i and output column j ,

$$((QS)_\sigma)_{ij} = \sum_{t=1}^k Q_{\sigma(i),t} S_{tj} = \sum_{t=1}^k (Q_\sigma)_{it} S_{tj} = (Q_\sigma S)_{ij}.$$

Thus the two matrices are equal entrywise.

Theorem 3.3 (BR computes the same eigenvalues as conventional D&C in exact arithmetic). *Assume BR and conventional D&C use the same split tree, deflation decisions, column ordering, column signs, and secular-equation convention. In exact*

arithmetic, every internal BR merge constructs the same secular problem as conventional D&C, and the root eigenvalues returned by BR are identical to those returned by conventional D&C.

Proof. The proof is by induction over the merge tree. At leaves, BR solves the same leaf eigenproblem as conventional D&C and returns the requested rows of the same local eigenvector matrix. For an internal node, the induction hypothesis gives the same child spectra and the same requested child boundary rows. By Lemma 3.1, BR constructs the same z and therefore the same diagonal-plus-rank-one secular problem as conventional D&C. The local eigenvalues are therefore the same. By Lemma 3.2, the parent rows requested by ancestors can be computed from selected child rows without forming unrequested rows. Hence the induction hypothesis also holds for the parent boundary state. Applying the argument up to the root proves the claim.

3.2.2 Conditioned Error Propagation. BR removes storage and arithmetic associated with unrequested rows, but it still relies on the same local numerical ingredients as D&C, including secular equation solves, deflation handling, and products used to form selected rows. Our stability statement is therefore conditioned on standard local stability interfaces rather than a fresh proof of the full LAPACK-style secular solver.

Let \widehat{B}_v be the computed boundary state at node v . If the two child boundary-row errors satisfy

$$\left\| \widehat{\text{bhi}}_L - \text{bhi}_L \right\|_2 \leq \eta_L, \quad \left\| \widehat{\text{blo}}_R - \text{blo}_R \right\|_2 \leq \eta_R, \quad (9)$$

then the error in the constructed secular vector satisfies

$$\left\| \widehat{z} - z \right\|_2^2 = \left\| \widehat{\text{bhi}}_L - \text{bhi}_L \right\|_2^2 + \left\| \widehat{\text{blo}}_R - \text{blo}_R \right\|_2^2 \leq \eta_L^2 + \eta_R^2. \quad (10)$$

Thus BR does not amplify the child boundary error when forming z beyond the norm of the concatenation. The remaining local error is the error of the secular solve and the selected-row update. Section A gives the detailed conditioned proof, including compact delta reconstruction, pointwise-to-Frobenius bounds, selected-row rounding-error composition, and tree-level propagation.

3.3 Complexity

The relevant comparison is between values-only D&C paths, not between BR and the public QR/QL routine xSTERF. The public xSTEDC values-only interface may choose the low-workspace QR/QL path, whereas LAPACK's internal values-only D&C machinery, represented by DLAED0 (ICOMPQ=0), retains enough replay state for DLAEDA to reconstruct future merge vectors. BR targets this second point in the design space: it keeps the D&C merge and secular-solve structure, but changes the vector-derived state that is carried across levels.

We use a pass-count model to make the constant-factor difference explicit. A length- K linear pass is counted as K , and K such passes are counted as K^2 . For a merge with active rank K , both BR and internal values-only D&C solve the same K secular equations. We write this shared root-solving cost as $c_{\text{sec}}K^2$, where c_{sec} absorbs the secular solver's implementation-dependent iteration count and reduction cost. Lazy replay additionally reconstructs the current merge vector from stored transformation state; we denote this cost by $c_{\text{rep}}K^2$. It also reconstructs updated secular quantities and materializes dense local $K \times K$ vector state for later replay. Thus a non-root internal values-only D&C merge has the leading form

$$T_{\text{lazy}}(K) = (c_{\text{sec}} + c_{\text{rep}} + 4)K^2 + O(K),$$

where the constant term represents the remaining quadratic passes for updated-vector reconstruction and dense local secular-vector materialization.

BR removes the replay term and avoids writing a dense local secular-vector block, but it does not reduce the asymptotic cost of the secular root solves. At a non-root merge, BR streams each secular vector column through at most two selected boundary rows. In the same pass-count model,

$$T_{\text{BR,nonroot}}(K) = (c_{\text{sec}} + 4)K^2 + O(K).$$

At the root, no parent consumes boundary rows, so BR skips selected-row propagation and computes only the final secular roots:

$$T_{\text{BR,root}}(K) = c_{\text{sec}}K^2 + O(K).$$

For a balanced D&C tree with constant leaf size,

$$\begin{aligned} \sum_{\text{internal nodes}} K^2 &= 2n^2 + O(n), \\ \sum_{\text{non-root internal nodes}} K^2 &= n^2 + O(n). \end{aligned} \quad (11)$$

Substituting Eqs. (3.3)–(3.3) gives the leading merge-path costs

$$T_{\text{lazy}}(n) = (2c_{\text{sec}} + 2c_{\text{rep}} + 8)n^2 + O(n \log n),$$

and

$$T_{\text{BR}}(n) = (2c_{\text{sec}} + 4)n^2 + O(n \log n).$$

Thus the saved leading work is

$$T_{\text{lazy}}(n) - T_{\text{BR}}(n) = (2c_{\text{rep}} + 4)n^2 + O(n \log n).$$

This is a constant-factor reduction in the D&C merge path, not a reduction of eigenvalue computation below the $O(n^2)$ secular root-solving work.

The asymptotic gain is in storage. Conventional lazy-replay D&C stores dense local secular-vector blocks and replay metadata, yielding quadratic real workspace and $O(n \log n)$ integer metadata in LAPACK's internal values-only D&C path. BR stores pole arrays, compact secular data, local metadata, and only the selected boundary rows required by ancestors. The resulting auxiliary state is $O(n)$, excluding the

input tridiagonal arrays and output eigenvalues. The implementation section uses this result as a contract: preserve the standard D&C merge semantics, but make boundary rows and compact secular data the only persistent eigenvector-derived state.

4 Implementation

The GPU and CPU code paths implement the same algorithmic modification to tridiagonal D&C. Both preserve the standard split tree, deflation, sorting, secular solves, and denominator reconstruction, but replace persistent full-eigenvector or replay state with the boundary-row state from Section 3.2. They differ only in platform realization: the GPU path maps the same state contract to resident CUDA kernels, while the CPU path exposes it through a LAPACK-style prototype for controlled comparison with existing routines.

4.1 GPU Implementation

The GPU values-only path is implemented as a resident tridiagonal D&C solver. It is used only when eigenvectors are not requested; full-vector tridiagonal D&C, dense back transformation, and other EVD stages use separate paths. The solver builds the split tree on the GPU, solves leaf subproblems, extracts only the first and last eigenvector rows from each leaf, and then processes the D&C tree bottom-up. Merge tasks at the same level are independent, so each level is handled by batched CUDA kernels over all active merges. The persistent eigenvector-derived state is the boundary-row state, while split metadata, active-column maps, compact secular-root data, and temporary reduction buffers are stored in GPU workspace.

At each non-root merge, the GPU path constructs the rank-one update vector from child boundary rows,

$$z = [\text{bhi}(Q_L), \text{blo}(Q_R)].$$

The implementation then performs the standard D&C merge steps on GPU, which include sorting child eigenvalues, detecting negligible z_i , detecting close poles, applying the corresponding Givens rotations, compacting the active secular problem, and recording active/deflated column mappings. The values-only distinction is the scope of these updates. Permutations and rotations that would normally be applied to full eigenvector blocks are applied only to the selected boundary rows and the associated metadata. This keeps deflation consistent with the standard algorithm while avoiding full-vector state.

After deflation, the active secular problem has rank K . The root solve evaluates the eigenvalues of $D + \rho z z^T$ with CUDA kernels that parallelize both across roots and across the pole reductions inside each root. For large K , block-reduction kernels evaluate sums such as

$$\sum_i \frac{z_i^2}{d_i - \lambda}$$

and the associated rescaling quantities in parallel within a CUDA block. This is important near the upper levels of the merge tree, where real dense-derived tridiagonal inputs often have limited deflation and therefore large active rank.

For non-root merges, the parent boundary rows are produced by streaming secular eigenvector columns through the selected rows. For an active root λ_j , the secular vector has entries

$$y_j(i) = \frac{z_i/(d_i - \lambda_j)}{\|z/(d - \lambda_j)\|_2}.$$

Instead of materializing the dense $K \times K$ secular eigenvector block Y , the kernel directly computes

$$R_{\text{parent}}(:, j) = R_{\text{child}} y_j,$$

where R_{child} contains at most two selected rows. Thus each column update is reduced to two streamed dot products. At the root, no parent will consume boundary rows, so the implementation switches to a root-only mode that computes the final secular roots and skips boundary-row propagation entirely.

The GPU implementation also avoids a dense $K \times K$ denominator matrix. Each secular root is stored in a compact representation consisting of an origin pole, an offset τ , and the near-pole denominator entries most sensitive to cancellation. Conceptually,

$$\lambda_j = d_{\text{origin}} + \tau_j, \quad \delta_i = d_i - d_{\text{origin}} - \tau_j.$$

During selected-row propagation, the kernel reconstructs each secular vector column from this compact state and uses the cached near-pole denominators where direct subtraction would lose relative accuracy. This preserves the stable denominator representation needed for secular-vector reconstruction while keeping the temporary state linear in the active merge size.

Overall, the GPU realization removes the persistent dense eigenvector matrix, dense secular eigenvector blocks, and replayable transformation history from the tridiagonal D&C stage. The algorithmic state remains the standard D&C secular problems and deflation metadata, but the vector-derived state is reduced to boundary rows. The CPU realization below follows the same state discipline in a LAPACK-compatible setting, which gives a controlled experimental vehicle for isolating the tridiagonal-stage behavior evaluated in Section 5.

4.2 CPU Implementation

The CPU prototype implements the same boundary-row algorithm as a private LAPACK-style path, `DSTEDC_DC_BR`. It deliberately does not change the public `DSTEDC('N')` behavior, which continues to use the standard low-memory QR/QL path. The private driver preserves the usual outer structure of a tridiagonal eigensolver: it validates arguments, splits at negligible off-diagonal entries, scales unreduced blocks, calls `DSTERF` for small blocks, and routes larger blocks to `DLAED0_BR`. This gives a controlled LAPACK-compatible

baseline for evaluating boundary-row D&C without changing public routine semantics.

DLAED0_BR keeps the standard D&C tree and stores two arrays, BLO and BHI, for the first and last rows of each active local eigenvector block. Leaf blocks are solved with DSTEQR('I'), but only these two rows are copied into persistent state. DLAED7_BR performs a single merge, DLAED8_BR mirrors LAPACK's sorting, deflation, permutation, and close-pole rotation logic on selected rows, and DLAED9_BR streams secular columns through those rows. DLAED4_BR provides the same compact denominator representation used by the GPU path, so the CPU implementation avoids storing full $K \times K$ denominator columns while retaining near-pole entries.

The CPU path exposes OpenMP parallelism without adding thread-dependent workspace. DLAED0_BR parallelizes independent merge pairs at the same tree level; each merge receives a scratch slice based on its physical interval, so same-level merges use disjoint workspace. For the root-only merge, independent secular root solves are parallelized using existing $O(K)$ scratch slices as per-thread denominator buffers. The large-block workspace query is $16N$ double-precision entries and $7N$ integer entries. In comparison, LAPACK's internal values-only D&C path DLAED0(ICOMPQ=0) requires $1 + 3N + 2N\lceil \log_2 N \rceil + 3N^2$ real workspace and $6 + 6N + 5N\lceil \log_2 N \rceil$ integer workspace. Thus the CPU boundary-row path reduces the leading real workspace term from $O(N^2)$ to $O(N)$ and removes the $O(N \log N)$ integer replay metadata.

The CPU implementation therefore closes the loop from the method to measurement: it keeps the same D&C merge semantics as the internal values-only D&C baseline, exposes OpenMP parallelism without thread-dependent persistent storage, and reports an explicit linear workspace query that can be checked directly in experiments.

5 Experiments

The preceding sections make three claims about BR: it should preserve the D&C merge semantics, replace persistent values-only D&C replay state with linear-size boundary data, and expose more parallelism than the low-memory QR/QL path when the spectrum permits useful deflation. This section tests those claims as one evidence chain. We first measure workspace and runnable scale, then compare against CPU QR/QL and internal values-only D&C baselines, and finally test the same values-only D&C design point against `cusolver` on an H100. Dense reduction and back transformation are outside the measured kernel because BR changes the tridiagonal D&C stage rather than the surrounding dense EVD pipeline.

5.1 Experimental Setup

All CPU experiments were run on one full compute node with two Intel Xeon Gold 6348 sockets, 28 physical cores per socket, and 56 cores in total. The jobs requested 56 CPU slots and 64 GB of memory from the scheduler. The code was compiled with `gfortran -O2 -fopenmp -std=legacy` and linked against Intel oneAPI MKL 2025.3 through `mk1_rt`. We set `OMP_PROC_BIND=close`, `OMP_PLACES=cores`, disable MKL dynamic threading, and use the LP64 GNU-threaded MKL runtime. For BR-only timing runs, `MKL_NUM_THREADS=1` so that the measured parallelism comes from the private BR OpenMP implementation rather than from nested MKL calls.

GPU experiments were run on one NVIDIA H100 PCIe GPU with 80 GB of device memory and CUDA 13.2. The scheduler job requested one `h100_pcie` GPU, eight CPU cores, and 80 GB of host memory. We use our GPU EVD prototype and build the tridiagonal D&C benchmark for SM90. The GPU benchmark runs the values-only tridiagonal D&C stage with `-backend=2`, `-vectors=0`, `-run-self=1`, and `-run-cusolver=1`; it therefore measures the same D&C stage targeted by BR rather than a full dense EVD pipeline. The synthetic and structured GPU rows use two warmup iterations and five timed iterations.

The CPU experiments use two fixed-seed pseudo-random tridiagonal families and two deterministic structured stress cases. The *uniform* family uses $d_i \sim U[-1, 1]$ and $e_i \sim U[0.10, 0.30]$. The *normal* family uses $d_i \sim \mathcal{N}(0, 1)$ and the same positive uniform off-diagonal distribution. Both pseudo-random families use a fixed xorshift seed determined by the distribution and N , so every matrix is exactly reproducible. The *Toeplitz* family uses constant entries $d_i = 2$ and $e_i = 0.25$. The *clustered* family uses nearly equal diagonal entries $d_i = 1 + 10^{-12}(i - (n + 1)/2)$ and small off-diagonal entries $e_i = 10^{-4}(1 + 0.1 \cos(0.33i))$. For the reduced-dense case, the H100 first reduces a dense symmetric input to tridiagonal form and writes only the compact D/E arrays; the CPU then reads that cache and measures only the tridiagonal eigensolver stage.

Timing reports the best elapsed time over repeated runs for small sizes and a single run for large sizes, matching the benchmark scripts. Accuracy is measured against DSTERF whenever a DSTERF reference was computed; for sizes beyond the reference range we report successful completion and checksums rather than claiming a reference error. We use normalized accuracy metrics,

$$e_{\text{fwd}} = \frac{\|\widehat{\lambda} - \lambda_{\text{ref}}\|_{\infty}}{\max(1, \|\lambda_{\text{ref}}\|_{\infty})}, \quad (12)$$

$$e_{\text{bwd}} = \frac{\|\widehat{\lambda} - \lambda_{\text{ref}}\|_{\infty}}{\max(1, \|T\|_{\infty})}. \quad (13)$$

The second quantity is a backward-error certificate scaled by the input tridiagonal norm. Raw absolute eigenvalue differences are omitted because they depend directly on the

spectrum scale. All memory numbers use the workspace query returned by the BR routine, which is $16N$ double entries and $7N$ integer entries for large blocks.

5.2 Baselines

We compare BR with two CPU baselines. The first baseline is LAPACK/MKL DSTERF, the standard eigenvalue-only QR/QL routine. It has very small storage requirements, essentially the diagonal and off-diagonal arrays, but exposes limited parallelism. The second baseline is the internal values-only D&C path, represented by the LAPACK-style DLAED0 (ICOMPQ=0) machinery in MKL. This path is the closest algorithmic comparison for BR because it preserves D&C secular merges and returns eigenvalues only, but it carries replay state for merge-vector reconstruction and therefore has much larger workspace. We use the term *internal values-only D&C* consistently for this baseline, rather than treating it as a public solver interface. The standard LP64 measurements cover this path through $N = 16,384$; selected ILP64 measurements extend the comparison to larger rows whose queried LWORK exceeds the LP64 integer range. On the GPU we compare against cuSOLVER `cusolverDnXstедc` with `compz=N`, the public cuSOLVER tridiagonal D&C interface for eigenvalues only.

5.3 Workspace and Scale

This workspace result is a design-space change, not a claim that BR uses less memory than QR/QL. DSTERF is the lowest-memory eigenvalue-only baseline: it stores only the tridiagonal arrays and therefore remains the right reference point when memory is the only objective. BR deliberately spends a larger, but still linear, workspace budget to recover the D&C merge parallelism without carrying dense eigenvector replay state. In production-style storage, the tridiagonal input plus BR workspace is about $172N$ bytes: D/E , $\text{WORK}(16N)$ in double precision, and $\text{IWORK}(7N)$ in 32-bit integers. This is about $10.75\times$ the QR/QL input storage, but it is still $O(N)$; the internal values-only D&C baseline, in contrast, has a quadratic real-workspace term.

Table 1 summarizes this trade-off at a shared reference size, $N = 65,536$, on the fixed-seed uniform family. At this size, QR/QL needs only about 1.00 MiB for D/E , but takes 56.52 s. BR uses 9.75 MiB of queried workspace and takes 10.56 ms on 56 threads. The internal values-only D&C formula would require about 96.0 GiB of real workspace at the same N , so we report it as OOM in the standard LP64 experiment. Table 3 separately includes ILP64 internal-D&C rows at $N = 32,768$ and on the reduced-dense input to show the cost once the interface limit is removed. The scale limit for BR in the current LP64 build is not node memory but the 32-bit LWORK count: BR successfully ran $N = 134,000,000$, within 0.2% of the bound $\lfloor (2^{31} - 1)/16 \rfloor$.

Table 1. Workspace design points at $N = 65,536$ on the fixed-seed uniform family. QR/QL is the lowest-memory baseline; BR uses more linear workspace to expose D&C parallelism, while internal values-only D&C is quadratic.

Path	Space	Mem. at 65,536	Time at 65,536
DSTERF / QR-QL	$O(N)$ input only	1.00 MiB	56.52 s
BR, 56T	$O(N)$ D&C state	9.75 MiB	10.56 ms
Internal values-only D&C	$O(N^2)$ replay state	96.0 GiB	OOM

Table 2. CPU comparison against DSTERF. Larger ratios mean BR is faster. The reduced-dense row uses D/E arrays produced once by GPU dense-to-tridiagonal reduction; timings exclude that shared reduction and measure only the tridiagonal eigensolver.

Input	N	DSTERF	BR 1T	BR 56T
<i>Fixed-seed pseudo-random</i>				
Uniform	16,384	4.17 s	79.2×	1330.8×
Uniform	65,536	56.52 s	262.2×	5351.1×
Normal	16,384	3.48 s	80.8×	1331.2×
Normal	65,536	48.85 s	274.9×	4378.1×
<i>Structured stress cases</i>				
Toeplitz	16,384	3.40 s	1.58×	3.99×
Toeplitz	65,536	51.94 s	1.58×	4.03×
Clustered	16,384	3.27 s	0.84×	3.00×
Clustered	32,768	12.76 s	0.83×	6.75×
<i>Reduced dense</i>				
Reduced dense	49,152	29.85 s	0.95×	8.06×

5.4 Performance Against QR/QL

BR is much faster than DSTERF on the fixed-seed pseudo-random families, and it still gives useful threaded speedups on the harder structured spectra and on a dense-derived tridiagonal input. Table 2 reports these CPU cases together so that the reader can compare the same baseline, metric, and thread count across input families. At $N = 65,536$, 56-thread BR is 5351× faster than DSTERF on uniform inputs and 4378× faster on normal inputs. On Toeplitz and clustered inputs, single-thread BR is not the right comparison point because both algorithms are close to quadratic; the threaded BR path is the useful one, giving about 4.0× on Toeplitz and 6.7× on the largest updated clustered row.

The reduced-dense row connects this tridiagonal study back to a dense EVD pipeline without charging either CPU solver for dense reduction. A GPU job first reduces a 49152×49152 dense symmetric matrix to tridiagonal form, stores the compact D/E arrays, and discards the dense intermediate. The CPU then solves exactly those cached arrays: single-thread BR is slightly slower than DSTERF, but the parallel BR path recovers an 8.06× speedup at 56 threads with the current root-solve scheduling. This result supports the intended hybrid usage: dense reduction can run on the GPU, while the compact tridiagonal stage remains transferable and can still benefit from BR on CPU.

The speedup comes from a change in empirical scaling on the pseudo-random families. For $N \geq 65,536$, uniform BR fits $N^{1.040}$ on one thread and $N^{0.973}$ on 56 threads, while normal BR fits $N^{1.033}$ and $N^{0.950}$, respectively. Over the referenced range $N = 4096$ to $65,536$, DSTERF fits approximately $N^{1.916}$ on uniform inputs and $N^{1.907}$ on normal inputs. This should be read as an empirical property of the measured spectra, not as an asymptotic proof that BR makes all tridiagonal eigenvalue problems linear.

5.5 Comparison with Internal D&C

The closest CPU D&C baseline is MKL’s internal values-only path that calls `DLAED0(ICOMPQ=0)`. This path has the same eigenvalue-only output as BR and uses the same secular-merge family, but it keeps the replay state needed to reconstruct merge vectors. Table 3 reports this comparison on the fixed-seed pseudo-random families, where BR has near-linear empirical scaling in Table 2. With one thread, BR is 3.1–3.8× faster than the internal values-only D&C path through $N = 16,384$, while using 2.44 MiB rather than 6.0 GiB of workspace. At $N = 32,768$, ILP64 internal-D&C runs require about 24.0 GiB, whereas BR still uses 4.88 MiB.

The multithreaded rows show that the remaining CPU gap was an implementation bottleneck rather than a necessary cost of the BR formulation. The leaf eigenproblems are independent, but an earlier prototype initialized them serially with `DSTEQR('I')`; parallelizing those leaf solves removes the dominant cost on pseudo-random inputs where later merge levels deflate strongly. At $N = 16,384$, BR is 4.38× faster than internal values-only D&C on uniform inputs and 3.43× faster on normal inputs, while preserving the same linear workspace advantage. The structured and reduced-dense cases show that this advantage is not limited to pseudo-random spectra: on 56 threads, BR is 3.79× faster on the ILP64 Toeplitz row and 6.13× faster on the ILP64 clustered row at $N = 32,768$, and 5.63× faster on the dense-derived tridiagonal input. The larger internal-D&C rows use ILP64 calls because their queried `LWORK` exceeds the LP64 integer range; their eigenvalues are checked against DSTERF with the same normalized forward- and backward-error metrics used for BR. Thus the internal-D&C evidence supports BR as both a state-reduction result and a practical faster values-only D&C path on the measured runnable cases.

5.6 GPU D&C Against cuSOLVER

The H100 experiment tests whether the same values-only state reduction is useful in a GPU D&C setting. Table 4 compares our GPU EVD prototype’s values-only D&C path with cuSOLVER `Xstedc` on the same tridiagonal inputs. The comparison is intentionally DC-only: both paths start from D/E , compute eigenvalues only, and exclude dense reduction and back transformation. For the reduced-dense row, a dense symmetric input is first reduced to tridiagonal form; the

Table 3. BR versus MKL internal values-only D&C. The internal path calls `DLAED0(ICOMPQ=0)` and is output-equivalent to BR. Ratios are internal/BR, so values above one mean BR is faster. Rows at $N = 32,768$ and the reduced-dense row use ILP64 internal-D&C calls when the LP64 `LWORK` count is insufficient.

Mode	N	Int. WS	BR WS	Int. Time	BR Time	Int./BR
<i>1-thread fixed-seed pseudo-random inputs</i>						
Uniform	4,096	386 MiB	0.61 MiB	41.4 ms	13.2 ms	3.15×
Uniform	8,192	1.50 GiB	1.22 MiB	83.8 ms	27.0 ms	3.10×
Uniform	16,384	6.01 GiB	2.44 MiB	173.9 ms	54.4 ms	3.20×
Uniform	32,768	24.0 GiB	4.88 MiB	369.8 ms	105.9 ms	3.49×
Normal	4,096	386 MiB	0.61 MiB	40.0 ms	10.5 ms	3.81×
Normal	8,192	1.50 GiB	1.22 MiB	80.5 ms	21.3 ms	3.77×
Normal	16,384	6.01 GiB	2.44 MiB	166.3 ms	43.4 ms	3.84×
Normal	32,768	24.0 GiB	4.88 MiB	332.0 ms	89.2 ms	3.72×
<i>56-thread ratio on runnable internal-D&C rows</i>						
Uniform	16,384	6.01 GiB	2.44 MiB	15.6 ms	3.57 ms	4.38×
Normal	16,384	6.01 GiB	2.44 MiB	11.0 ms	3.20 ms	3.43×
Toeplitz	16,384	6.01 GiB	2.44 MiB	3.04 s	812 ms	3.75×
Clustered	16,384	6.01 GiB	2.44 MiB	5.80 s	972 ms	5.97×
Toeplitz	32,768	24.0 GiB	4.88 MiB	11.90 s	3.14 s	3.79×
Clustered	32,768	24.0 GiB	4.88 MiB	23.27 s	3.80 s	6.13×
Reduced dense	49,152	54.0 GiB	7.31 MiB	44.8 s	7.95 s	5.63×

shared preparation time is excluded, so the row still measures only the D&C solver stage.

The results show two effects. First, cuSOLVER’s queried device workspace grows quadratically and reaches 54.0 GiB at $N = 49152$, while our GPU EVD prototype uses a compact D/E cache and a 4096-column temporary slab, about 1.5 GiB for the largest case. This is the GPU form of the state-management issue addressed by BR: even before full dense EVD is considered, the public D&C path carries a large workspace.

Second, after removing a serial split-metadata update from the GPU path, our GPU EVD prototype is faster than cuSOLVER on every measured $N = 49152$ row in Table 4. On the fixed-seed pseudo-random inputs, the speedups are 1.86× for normal and 1.74× for uniform. The dense-derived and structured rows show larger gains: 2.60× on the reduced-dense tridiagonal input, 5.73× on Toeplitz, and 3.57× on clustered inputs. Thus the GPU data supports the same interpretation as the CPU data. BR makes a much lower-memory D&C design point available, and the speedups are largest when conventional D&C moves substantially more state than the boundary-row path needs.

Profiling explains why the pseudo-random speedups are smaller than the structured ones. Before the split-metadata fix, a serial split-update kernel consumed about 72 ms at $N = 49152$ on normal and uniform inputs, larger than the secular root-solving time. Parallelizing this metadata update reduces the split-update cost to microsecond-scale overhead. The remaining dominant kernels are boundary-vector construction, about 42 ms, and local eigenvalue sorting, about

Table 4. H100 values-only tridiagonal D&C comparison with cuSOLVER Xstedc. Larger cuSOLVER/ours ratios mean our GPU EVD prototype is faster.

Mode	N	Our GPU EVD	cuSOLVER	cuSOLVER/ours
Normal	49,152	78.73 ms	146.71 ms	1.86×
Uniform	49,152	85.75 ms	149.09 ms	1.74×
Reduced dense	49,152	683.18 ms	1.78 s	2.60×
Toeplitz	49,152	480.81 ms	2.75 s	5.73×
Clustered	49,152	697.22 ms	2.49 s	3.57×

15 ms. These costs are mostly per-level D&C bookkeeping rather than secular arithmetic, so they are most visible on pseudo-random spectra where deflation makes the root solves relatively cheap.

5.7 Effect of Spectrum Structure

The spectrum strongly affects the observed speedup, which is why the paper reports pseudo-random and structured cases together. The uniform and normal families have substantial deflation and produce near-linear BR timings in the measured large- N range. Toeplitz and clustered families are harder: for $N \geq 4096$, both DSTERF and BR fit close to quadratic growth. The Toeplitz fits are $\text{DSTERF} \propto N^{1.972}$, $\text{BR } 1\text{T} \propto N^{1.975}$, and $\text{BR } 16\text{T} \propto N^{1.930}$ over the available 16-thread range. The clustered fits are similarly quadratic, with $\text{DSTERF} \propto N^{1.953}$, $\text{BR } 1\text{T} \propto N^{1.979}$, and $\text{BR } 16\text{T} \propto N^{1.941}$. In these harder cases, BR should be described as a lower-memory D&C formulation with useful constant-factor and threading benefits, not as a universally growing-speedup replacement for QR/QL.

This caveat is important for interpreting the main result. BR removes dense eigenvector-derived state from values-only D&C and exposes more parallelism than DSTERF; it does not remove the secular root-solving work that remains when deflation is weak. The measurements therefore support a conditional performance claim: BR is especially effective for spectra where D&C deflation and selected-row propagation keep the merge work close to linear, while its most general guarantee is linear auxiliary storage.

5.8 Numerical Accuracy

For all benchmark rows with a DSTERF reference, BR produced eigenvalues close to the reference under the normalized metrics defined above. The fixed-seed pseudo-random cross-checks cover uniform and normal diagonal distributions through $N = 65,536$, while the structured checks cover Toeplitz, clustered, and reduced-dense tridiagonal inputs. We report forward and backward errors rather than raw eigenvalue differences so that the reduced-dense case, whose spectrum has $\|\lambda\|_\infty = 4.93 \times 10^4$, is compared on the same scale as the synthetic cases. These normalized checks are consistent with the conditioned-error argument in Section 3.2.2: BR changes which rows are propagated, but it uses the same

local secular-equation ingredients as D&C and constructs the same merge vectors in exact arithmetic.

6 Conclusion

This paper presents boundary-row D&C, a values-only tridiagonal eigensolver that keeps the parallel D&C merge structure while removing the dense eigenvector-derived state that makes conventional values-only D&C memory-heavy. The central idea is to propagate only the boundary rows needed by future rank-one merges. This state is sufficient to construct the same secular problems as conventional D&C in exact arithmetic, reduces persistent auxiliary storage from quadratic to linear, and maps naturally to both CPU and GPU implementations.

The prototypes show the practical effect of this reduced state. On CPUs, BR reaches problem sizes near the LP64 workspace limit and reduces the internal values-only D&C state from quadratic replay storage to linear boundary-row storage. This is not a claim that BR uses less memory than QR/QL, which remains the minimal-storage eigenvalue-only baseline; rather, BR keeps D&C-style parallelism while avoiding the quadratic state of conventional values-only D&C. With parallel leaf initialization, the CPU BR prototype is faster than both DSTERF and MKL’s internal D&C path on the completed pseudo-random and structured rows. ILP64 internal-D&C runs confirm that larger cases can be executed when the interface and memory budget allow it, but the quadratic replay state remains expensive: $N = 32,768$ already requires about 24.0 GiB, and BR remains faster on the completed ILP64 rows. On an H100, the values-only D&C path avoids the large quadratic cuSOLVER workspace and is faster than cuSOLVER on all measured $N = 49152$ tridiagonal-stage cases, with 1.74–5.73× speedups on the synthetic and structured families after parallelizing split-metadata updates.

These results make the boundary clear. BR is not a universal subquadratic eigensolver; it makes the D&C design point available to eigenvalue-only workloads without carrying full eigenvector state.

References

- [1] Hervé Abdi and Lynne J Williams. 2010. Principal component analysis. *Wiley interdisciplinary reviews: computational statistics* 2, 4 (2010), 433–459.
- [2] Edward Anderson, Zhaojun Bai, Christian Bischof, L Susan Blackford, James Demmel, Jack Dongarra, Jeremy Du Croz, Anne Greenbaum, Sven Hammarling, Alan McKenney, et al. 1999. *LAPACK Users’ guide*. SIAM.
- [3] Paolo Bientinesi, Inderjit S Dhillon, and Robert A Van De Geijn. 2005. A parallel eigensolver for dense symmetric matrices based on multiple relatively robust representations. *SIAM Journal on Scientific Computing* 27, 1 (2005), 43–66.
- [4] J. J. M. Cuppen. 1981. A divide and conquer method for the symmetric tridiagonal eigenproblem. *Numer. Math.* 36 (1981), 177–195.
- [5] RZ Dautov, AD Lyashko, and SI Solov’ev. 1994. The bisection method for symmetric eigenvalue problems with a parameter entering nonlinearly. (1994).

- [6] Inderjit S Dhillon and Beresford N Parlett. 2004. Multiple representations to compute orthogonal eigenvectors of symmetric tridiagonal matrices. *Linear Algebra Appl.* 387 (2004), 1–28.
- [7] Gene H Golub and Charles F Van Loan. 2013. *Matrix computations*. JHU press.
- [8] Roger Grimes, Henry Krakauer, John Lewis, Horst Simon, and Su-Hai Wei. 1987. The solution of large dense generalized eigenvalue problems on the Cray X-MP/24 with SSD. *J. Comput. Phys.* 69, 2 (1987), 471–481.
- [9] Ming Gu and Stanley C Eisenstat. 1994. A stable and efficient algorithm for the rank-one modification of the symmetric eigenproblem. *SIAM journal on Matrix Analysis and Applications* 15, 4 (1994), 1266–1276.
- [10] Ming Gu and Stanley C Eisenstat. 1995. A divide-and-conquer algorithm for the symmetric tridiagonal eigenproblem. *SIAM J. Matrix Anal. Appl.* 16, 1 (1995), 172–191.
- [11] Vineet Gupta, Tomer Koren, and Yoram Singer. 2018. Shampoo: Pre-conditioned stochastic tensor optimization. In *International Conference on Machine Learning*. PMLR, 1842–1850.
- [12] MAGMA Project. 2026. *MAGMA 2.10.0 Documentation: Symmetric/Hermitian Eigenvalue Drivers*. University of Tennessee, Knoxville. https://icl.utk.edu/projectsfiles/magma/doxygen/group__magma__heevd.html.
- [13] MAGMA Project. 2026. MAGMA Source Code: dsyevd.cpp, dsyevd_gpu.cpp, and dstedx.cpp. <https://github.com/icl-utk-edu/magma/tree/master/src>.
- [14] A Melman. 1995. Numerical solution of a secular equation. *Numer. Math.* 69 (1995), 483–493.
- [15] NVIDIA Corporation. 2026. *NVIDIA cuSOLVER Documentation*. NVIDIA Corporation. <https://docs.nvidia.com/cuda/cusolver/>.
- [16] Matt Probert. 2011. *Electronic Structure: Basic Theory and Practical Methods*, by Richard M. Martin: Scope: graduate level textbook. Level: theoretical materials scientists/condensed matter physicists/computational chemists.
- [17] Notker Rösch, Sven Krüger, Vladimir A Nasluzov, and Alexei V Matveev. 2005. ParaGauss: The density functional program paragauss for complex systems in chemistry. In *High Performance Computing in Science and Engineering, Garching 2004*. Springer, 285–296.
- [18] Ruchi Shah, Shaoshuai Zhang, Ying Lin, and Panruo Wu. 2019. xSVM: Scalable distributed kernel support vector machine training. In *2019 IEEE International Conference on Big Data (Big Data)*. IEEE, 155–164.
- [19] Françoise Tisseur and Jack Dongarra. 1999. A parallel divide and conquer algorithm for the symmetric eigenvalue problem on distributed memory architectures. *SIAM Journal on Scientific Computing* 20, 6 (1999), 2223–2236.
- [20] Stanimire Tomov, Rajib Nath, Peng Du, and Jack Dongarra. 2011. *MAGMA Users’ Guide. ICL, UTK (November 2009)* (2011).
- [21] Hansheng Wang, Zhekai Duan, Zitian Zhao, Siqi Wu, Saiqi Zheng, Qiao Li, Xu Jiang, and Shaoshuai Zhang. 2025. Improving Tridiagonalization Performance on GPU Architectures. In *Proceedings of the 30th ACM SIGPLAN Annual Symposium on Principles and Practice of Parallel Programming*. 469–480.
- [22] David S Watkins. 1982. Understanding the QR algorithm. *SIAM review* 24, 4 (1982), 427–440.
- [23] Shaoshuai Zhang, Ruchi Shah, and Panruo Wu. 2020. TensorSVM: accelerating kernel machines with tensor engine. In *Proceedings of the 34th ACM International Conference on Supercomputing*. 1–11.

A Proof Details

This appendix records the BR-specific algebra and conditioned error-propagation details used by Section 3.2.2. It does not reprove the stability of a complete secular-equation solver, nor does it formalize all IEEE 754 behavior. Those

components are treated as external numerical-analysis assumptions.

A.1 Conventions

For a local eigenvector block $Q \in \mathbb{R}^{m \times n}$, define

$$\text{blo}(Q) = Q_{1,:}, \quad \text{bhi}(Q) = Q_{m,:}.$$

The boundary state is $B(Q) = (\text{blo}(Q), \text{bhi}(Q))$. A secular problem is written as

$$P = (D, z, \rho), \quad A(P) = \text{diag}(D) + \rho z z^T,$$

where D is the pole vector and ρ carries the rank-one strength. For perturbation bookkeeping we use

$$\left\| \widehat{P} - P \right\|_p = \left(\left\| \widehat{D} - D \right\|_2^2 + \|\widehat{z} - z\|_2^2 + |\widehat{\rho} - \rho|^2 \right)^{1/2}.$$

This unweighted norm can be replaced by a weighted norm; the corresponding perturbation constants then absorb the scaling of D , z , and ρ .

A.2 Row Selection and Metadata

Lemma A.1 (Column permutations commute with row selection). *Let Π be a column permutation matrix and let σ be an arbitrary row list. Then*

$$(Q\Pi)_\sigma = Q_\sigma\Pi.$$

Proof. For every requested row i and column j , both sides equal $Q_{\sigma(i),\pi(j)}$.

Lemma A.2 (Local rotations commute with row selection). *Let G be a Givens rotation or any other right-multiplied local column transformation. Then*

$$(QG)_\sigma = Q_\sigma G.$$

Proof. This is the same entrywise argument as Lemma 3.2; a Givens rotation changes only two columns, and every affected entry is a fixed linear combination of the two selected-row entries.

In an implementation, column signs, deflation-induced permutations, and sorting metadata must be applied consistently to both conventional D&C and BR. Equivalently, one may regard the stored state as

$$B(Q, \pi, s) = (s \odot Q_{1,\pi}, s \odot Q_{m,\pi}),$$

where π is a column permutation and s is a column-sign convention. Under this convention, the algebraic equality in Theorem 3.3 is exact.

A.3 Compact Delta Reconstruction

For a secular root written as $\lambda = D_{\text{org}} + \tau$, define

$$\Delta_i = D_i - D_{\text{org}} - \tau.$$

Near-pole entries may be cached to avoid cancellation, while far entries are reconstructed by the formula above.

Lemma A.3 (Compact delta correctness). *Assume the compact representation has legal near indices, non-near indices equal the complement of the cached near set, and cached near entries equal the corresponding exact Δ_i . If every non-near entry is reconstructed as $D_i - D_{\text{org}} - \tau$, then the reconstruction returns the exact vector Δ in exact arithmetic.*

Proof. For a near index, the returned value is the cached exact entry. For a non-near index, the returned value is exactly the defining formula for Δ_i . Thus all entries match.

Lemma A.4 (Pointwise delta error to vector error). *If $|\widehat{\Delta}_i - \Delta_i| \leq \eta$ for all i , then*

$$\|\widehat{\Delta} - \Delta\|_2 \leq \sqrt{n} \eta.$$

Proof. Square the pointwise bound, sum over i , and take square roots.

Lemma A.5 (Far-entry absolute rounding bound). *Let a far entry be computed as*

$$\widehat{\Delta}_i = \text{fl}(\text{fl}(\widehat{D}_i - \widehat{D}_{\text{org}}) - \widehat{\tau}),$$

and assume $\text{fl}(x - y) = (x - y)(1 + \delta)$ with $|\delta| \leq u$. If

$$|\widehat{D}_i - D_i| \leq \eta_D, \quad |\widehat{D}_{\text{org}} - D_{\text{org}}| \leq \eta_D, \quad |\widehat{\tau} - \tau| \leq \eta_\tau,$$

then

$$|\widehat{\Delta}_i - \Delta_i| \leq u|\widehat{D}_i - \widehat{D}_{\text{org}}| + u|\text{fl}(\widehat{D}_i - \widehat{D}_{\text{org}}) - \widehat{\tau}| + 2\eta_D + \eta_\tau.$$

Proof. Let $a = \widehat{D}_i - \widehat{D}_{\text{org}}$ and $b = \text{fl}(a) - \widehat{\tau}$. Then

$$|\widehat{\Delta}_i - \Delta_i| \leq |\text{fl}(b) - b| + |b - \Delta_i| \leq u|b| + u|a| + 2\eta_D + \eta_\tau.$$

Substituting a and b gives the result.

This is an absolute error bound. A relative bound for far entries requires a separation condition such as

$$|\Delta_i| \geq \alpha (|D_i - D_{\text{org}}| + |\tau|),$$

for a positive constant α .

A.4 Selected-Row Rounding Error

Assumption A.1 (Dot-product error model). *For a length- k dot product, the implementation satisfies*

$$\left| \text{flDot}(x, y) - \sum_{t=1}^k x_t y_t \right| \leq \gamma_k \sum_{t=1}^k |x_t y_t|.$$

For sequential summation with $ku < 1$, one may take $\gamma_k = ku/(1 - ku)$.

Proposition A.6 (Selected-row update with input perturbation). *Let $Y = Q_\sigma S$ and let $\widehat{Y} = \text{flMatMul}(\widehat{Q}_\sigma, \widehat{S})$. If every output entry satisfies*

$$|\widehat{Y}_{ij} - (\widehat{Q}_\sigma \widehat{S})_{ij}| \leq \eta_{\text{round}},$$

and

$$|(\widehat{Q}_\sigma \widehat{S})_{ij} - (Q_\sigma S)_{ij}| \leq \eta_{\text{input}},$$

then

$$\|\widehat{Y} - Y\|_F \leq \sqrt{r\ell} (\eta_{\text{round}} + \eta_{\text{input}}),$$

where $Q_\sigma \in \mathbb{R}^{r \times k}$ and $S \in \mathbb{R}^{k \times \ell}$.

Proof. By the triangle inequality, every entry of $\widehat{Y} - Y$ is bounded by $\eta_{\text{round}} + \eta_{\text{input}}$. The Frobenius bound follows by summing the squared entrywise bounds over the $r\ell$ entries.

The dot-product model gives $\eta_{\text{round}} = \gamma_k M_{\text{abs}}$ whenever

$$\sum_{t=1}^k |(\widehat{Q}_\sigma)_{it} \widehat{S}_{tj}| \leq M_{\text{abs}}$$

for all actual dot products. This quantity must bound the sum of absolute products, not the cancellation-reduced exact dot product.

A.5 WPROD Product Chains

Some secular-vector entries are computed as products

$$W = W_0 \prod_{i=1}^m f_i.$$

Assume every effective factor satisfies

$$\widehat{f}_i = f_i(1 + \delta_i), \quad |\delta_i| \leq u.$$

Then

$$\widehat{W} = W(1 + \theta), \quad \theta = \prod_{i=1}^m (1 + \delta_i) - 1.$$

If $0 \leq u \leq 1$, then

$$|\theta| \leq \Gamma_m^\pm(u) = \max\{(1 + u)^m - 1, 1 - (1 - u)^m\}.$$

This proves only composition of relative factor perturbations; stability of the individual factor evaluations must be supplied separately.

A.6 Tree-Level Propagation

Theorem A.7 (Conditional boundary-error propagation).

Assume each leaf ℓ satisfies $\|\widehat{B}_\ell - B_\ell\| \leq E_\ell$. For every internal node v , assume the local merge routine has a declared output bound

$$\|\widehat{B}_v - B_v\| \leq F_v(\eta_L, \eta_R, \eta_D, \eta_\rho, \eta_{\text{round}}, \kappa_v) \equiv E_v,$$

whenever the left and right child boundary errors satisfy their input bounds. Then every node in the BR merge tree satisfies its declared bound. Moreover, every internal secular vector satisfies

$$\|\widehat{z}_v - z_v\|_2 \leq \sqrt{\eta_{L(v)}^2 + \eta_{R(v)}^2} \leq \eta_{L(v)} + \eta_{R(v)}.$$

Proof. The proof is induction on tree height. Leaf nodes satisfy the hypothesis. For an internal node, the induction hypothesis supplies the child boundary-error bounds. Equation (10) gives the secular-vector perturbation, and the assumed local merge bound gives $\|\widehat{B}_v - B_v\| \leq E_v$.

Theorem A.8 (Root values-only error decomposition). *Let $P = (D, z, \rho)$ be the exact root secular problem and \widehat{P} the BR-computed perturbed problem. If*

$$\left\| \widehat{P} - P \right\|_P \leq \eta_{\text{prob}},$$

and the local eigenvalue map obeys

$$\left\| \lambda(\widehat{P}) - \lambda(P) \right\|_2 \leq \kappa_{\text{pert}} \eta_{\text{prob}},$$

while the root solver obeys

$$\left\| \widehat{\lambda} - \lambda(\widehat{P}) \right\|_2 \leq \eta_{\text{solver}},$$

then

$$\left\| \widehat{\lambda} - \lambda(P) \right\|_2 \leq \eta_{\text{solver}} + \kappa_{\text{pert}} \eta_{\text{prob}}.$$

Proof. Apply the triangle inequality:

$$\left\| \widehat{\lambda} - \lambda(P) \right\|_2 \leq \left\| \widehat{\lambda} - \lambda(\widehat{P}) \right\|_2 + \left\| \lambda(\widehat{P}) - \lambda(P) \right\|_2.$$

The two terms are bounded by the solver and perturbation assumptions.

For a simplified balanced-tree model with per-level additive local error μ , the loose recurrence $E_{h+1} = 2E_h + \mu$ gives

$$E_h = 2^h \eta_0 + (2^h - 1)\mu.$$

Using the sharper concatenation bound gives $U_{h+1} = \sqrt{2}U_h + \mu$ and

$$U_h = (\sqrt{2})^h \eta_0 + \frac{(\sqrt{2})^h - 1}{\sqrt{2} - 1} \mu.$$

These recurrences are illustrative upper-bound models; the actual local Lipschitz constants and secular conditioning are contained in F_σ .